Coulomb Fission in Dielectric Dication Clusters: Experiment and Theory on Steps That May Underpin the Electrospray Mechanism

Xiaojing Chen,[†] Elena Bichoutskaia, and Anthony J. Stace*

Department of Physical and Theoretical Chemistry, School of Chemistry, University of Nottingham, University Park, Nottingham NG7 2RD, United Kingom

ABSTRACT: A series of five molecular dication clusters, $(H_2O)_n^{2+}$, $(NH_3)_n^{2+}$, $(CH_3CN)_n^{2+}$, $(C_5H_5N)_n^{2+}$, and $(C_6H_6)_n^{2+}$, have been studied for the purpose of identifying patterns of behavior close to the Rayleigh instability limit where the clusters might be expected to exhibit Coulomb fission. Experiments show that the instability limit for each dication covers a range of sizes and that on a time scale of 10^{-4} s ions close to the limit can undergo either Coulomb fission or neutral evaporation. The observed fission pathways exhibit considerable asymmetry in the sizes of the charged fragments, and are associated with kinetic (ejection) energies of ~0.9 eV. Coulomb fission has been modeled using a theory recently formulated to describe how charged particles of dielectric materials interact with one another (Bichoutskaia et al. *J. Chem. Phys.* **2010**, *133*, 024105). The calculated electrostatic interaction energy between separating fragments accounts for the observed asymmetric fragmentation and for the magnitudes of the measured ejection energies. The close match between theory and experiment suggests that a significant fraction of excess charge resides on the surfaces of the fragment ions. The experiments provided support for a fundamental step in the electrospray ionization (ESI) mechanism, namely the ejection from droplets of small solvated charge carriers. At the same time, the theory shows how water and acetonitrile may behave slightly differently as ESI solvents. However, the theory also reveals deficiencies in the point-charge image-charge model that has previously been used to quantify Coulomb fission in the electrospray process.
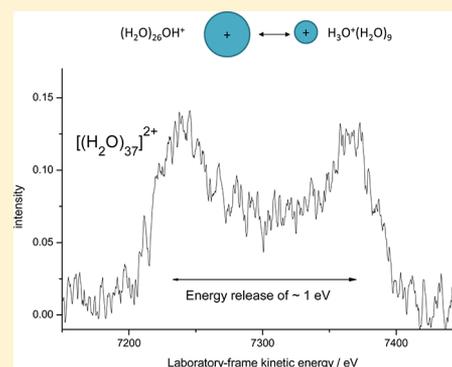
I. INTRODUCTION

There are notable parallels between existing qualitative experimental observations on multiply charged clusters[1−7] and attempts to identify mechanisms responsible for the appearance of multiply charged ions during electrospray ionization (ESI).[8−16] Both systems conform to the Rayleigh instability relationship, where the critical number of molecules required to stabilize a multiply charged droplet can be estimated from the classical liquid-drop equation: $(Qe)^2/n_{cr} = 64\pi^2\gamma\varepsilon_0\varepsilon_r r_0^3$, where Qe is the total charge, γ the surface tension, r_0 the radius of a constituent molecule, ε_0 the permittivity of free space, and ε_r the relative dielectric permittivity. For ESI droplets, Qe is the critical quantity, whereas for multiply charged clusters much of the discussion centers on n_{cr}, the minimum number of atoms or molecules required to accommodate two or more charges. Both droplets and clusters are considered unstable with respect to charge separation or Coulomb fission when the ratio $(Qe)^2/n_{cr}$ exceeds unity.[17] In experiments on multiply charged clusters, considerable effort has been devoted to identifying those patterns of behavior that might prevail at n_{cr};[1,4−6,18] Coulomb fission is the most obvious outcome, but definitive answers have not been forthcoming. Likewise, discussions on the final steps of the ESI process have focused on two mechanisms: in the charge residue model (CRM) highly charged ions, such as proteins, are thought to form as a result of extensive solvent evaporation, during which the ion of interest retains or acquires a significant fraction of the total available charge.[19,20] A second mechanism, the ion evaporation mechanism (IEM), is thought to proceed via the ejection of small solvated ions and appears to be more applicable to the appearance of relatively small residual ions.[21,22] It has been suggested that CRM and IEM models commence with a combination of evaporation and Coulomb fission, with any differentiation most likely to appear as they approach a final size.[8,9] The CRM and IEM mechanisms have both been discussed in detail in several recent reviews.[8,9,12]

Reported here are the first measurements of delayed Coulomb fission in a range of size-selected dication clusters comprising the following molecular species: $(H_2O)_n^{2+}$,[2] $(NH_3)_n^{2+}$,[23] $(CH_3CN)_n^{2+}$,[6] $(C_5H_5N)_n^{2+}$,[24] and $(C_6H_6)_n^{2+}$;[6,25] in each case, n is close in value to the Rayleigh instability limit that has been identified from previous experiments on these dications. The results show that molecular dication clusters can both eject small solvated ions and undergo the evaporation of neutral molecules but that these processes proceed in competition and over a range of sizes rather than at a unique critical size. To interpret the results, reaction potential energy surfaces for the subprocess that involves the ejection of solvated ions have been modeled by representing the fission products as charged dielectric spheres. These calculations have been undertaken using an analytical solution developed recently to solve the long-standing problem of how charged spheres of

dielectric materials interact with one another.[26] The results show how the electrostatic potential energy depends on the relative dielectric permittivity of the clusters and, for a fixed charge, the ratio of the sizes of their fragments.[26] Experimental measurements of the average center-of-mass kinetic energy (ejection energy) acquired by charged fragments as they separate, are a good match to the calculated heights of the reverse electrostatic barriers.

II. EXPERIMENTAL SECTION

Observations on the fragmentation patterns of molecular dication clusters have been made on an apparatus that consists of a high resolution reversed geometry mass spectrometer (VG Analytical ZAB-E) coupled with a supersonic expansion nozzle. The supersonic nozzle system consists of two differentially pumped chambers; an expansion chamber which houses a pulsed nozzle and a collimation chamber separated from the former by a 1 mm diameter skimmer. Clusters were generated by an expansion of gas or vapor/argon mixture through a 200 μm diameter conical nozzle, 5 mm in length and with an opening angle of 30°. The gas flow is pulsed by a Bosch fuel injector valve driven by a 0−12 V square wave pulse at a frequency of between 10 and 20 Hz. A 3 mm diameter cap, covered in a disc of Kalrez fitted onto the injector needle seals against the nozzle when the voltage pulse is low. To generate molecular clusters from liquids and vapors, argon was passed through the liquid contained in a reservoir cooled in an ice bath.

Neutral clusters in the beam were ionized by 70 eV electrons and the resulting ion beam was then extracted from the source at a potential of +5 kV into the flight tube of the mass spectrometer. Cluster ions with a particular combination of charge (Q_i) and mass (m_i) were selected using a magnet, and the ionic products of Coulomb fission in the field free region between the magnet and an electrostatic analyzer (ESA) were identified by scanning the voltage on the latter. The field-free region is 1.5 m in length, and ions are approximately 5×10^{-5} s old when they enter that section of the mass spectrometer. This link-scanning procedure provides a mass-analyzed ion kinetic energy (MIKE) spectrum,[27] which can be used to identify ionic fragments according to their laboratory-frame kinetic energy. To detect the principal singly charged products from the fission of a doubly charged cluster, the ESA was scanned to record ionic fragments with laboratory-frame kinetic energies from 10 keV downward. For laboratory-frame kinetic energies of between 5 and 10 keV there are no background ion signals from other processes, such as the loss of neutral molecules, which means the very weak signals that arise from Coulomb fission can be recorded without interference. However, this approach does mean that only the largest of the singly charged fragments is detected. The size of the smaller fragment is determined from mass balance and the assumption that it emerges as a single particle is supported by the shape of the peak profiles recorded for Coulomb fission.

From the magnitude of the electric sector voltage necessary to transmit them, the mass-to-charge ratio of fragment ions can be identified from the following equation:[27]

$$E^* = \frac{m_2}{m_i} \frac{Q_i}{Q_2} E_0 \tag{1}$$

E_0 is the initial parent ion kinetic energy (5000 eV in the present experiment), E^* is the kinetic energy after fragmenta-

tion, and m_2 and Q_2 are the mass and charge, respectively, of the fragment ion being detected. Ion detection was achieved via a Daly scintillation detector linked to a lock-in amplifier (Stanford Research Systems SR850), which provided phase-sensitive detection referenced with respect to the train of nozzle pulses. During the course of these experiments, the background pressure beyond the ion source remained less than 1×10^{-7} mbar, which ensured minimal interference from collision induced fragmentation.

III. THEORY

Charged particles in one form or another are ubiquitous, and in those instances where they interact with one another, the particles concerned are invariably composed of dielectric materials. However, it is only very recently that accurate analytical solutions have emerged to describe the electrostatic forces that exist between two such particles.[26,28] The electrostatic force due to the presence of a permanent free charge, Q_1 and Q_2, residing on the surfaces of two interacting spherical particles is given as a generalization of Coulomb's law for point charges:[26]

$$
\begin{aligned}
F_{12} &= K \int dQ_1(x_1) \int d(x_2) \frac{x_1 - x_2}{|x_1 - x_2|^3} \\
&= -\hat{z} \frac{\partial}{\partial h} \left(K \int dQ_1(x_1) \int dQ_2(x_2) \frac{1}{|x_1 - x_2|} \right) \Bigg|_{\sigma_{f,i}=\text{const}}
\end{aligned}
\tag{2}
$$

where x_1 and x_2 are points on spheres 1 and 2, $\hat{z}$ is a unit vector along the axis connecting the two spheres, h is their center-to-center separation and $K = 1/4\pi\varepsilon_0 \approx 9 \times 10^9$ V mC^{-1} is a constant of proportionality, where ε_0 is the permittivity of free space (8.8542×10^{-12} F m^{-1}). The first integral takes into account the charge residing on sphere 1, and the second integral is the potential generated by the charge residing on sphere 2. The last equality in eq 2 is due to the cylindrical symmetry of the problem and requires that differentiation of the electric potential with respect to h is performed with the free surface charge density, $\sigma_{f,i}$ ($i = 1, 2$) kept constant on both spheres. The electrostatic force, F_{12}, is evaluated by an expansion in Legendre polynomials of the electrical potential generated by the two spheres as they interact. The convention where F_{12} is negative for an attractive interaction and positive where the force is repulsive has been used, and the permittivity of a sphere is introduced as the dimensionless dielectric constant ε_i, which is taken as relative to that of a vacuum. Additional boundary conditions describe the behavior of the electrical potential and its continuity on the surfaces of the spheres.[26]

Each dielectric particle is assumed to be electrically neutral in its uncharged state with an equal number of positive and negative charges, which are bounded by the surface of the particle, and the surface density of this bound charge is defined as $\sigma_{b,i}$. The total surface charge density, σ_i, is, therefore, related to the free and bound charge densities by $\sigma_i = \sigma_{f,i} + \sigma_{b,i}$. The free charge on each particle is taken to be fixed, independent of the dielectric constant, and not to vary with separation between particles. It is also assumed that the density of free charge, $\sigma_{f,i}$, across the surface of a particle is uniform. In the absence of an external perturbation, such as an electric field, the bound surface charge on each particle is also assumed to be evenly distributed over the surface of a particle. Variations in electrostatic force acting on the system can arise as a result

of polarization of the bound surface charge density, $\sigma_{b,i}$, of one particle being induced by an electric field due to the presence of charge on a second particle. This redistribution of bound surface charge is represented by multipole terms that appear in expressions for the electrostatic force and interaction energy between particles. No volume charges are taken into account as the overall effects of their polarization in an external electric field cancel out.

In an earlier Communication,[29] where results were presented following a preliminary study of Coulomb fission in $(NH_3)_n{}^{2+}$ clusters, the data were interpreted using the dielectric particle model of Linse.[28] Subsequent to that work, Bichoutskaia et al.[26] presented a new analytical solution to eq 2 that exhibits rapid convergence and remains stable up to the point where particles touch. The latter solution is the subject of further discussion presented below and has also been used to interpret all of the new results presented in this paper.

An expression for the Coulomb interaction energy, U, between the two charged dielectric spheres has been given earlier,[26] and more efficient procedures, where matrix relationships can be used for calculating both the electrostatic force and the electrostatic interaction energy, have been presented elsewhere.[30] For the purpose of comparison with other approaches that have been used to model Coulomb fission and ion evaporation processes linked to electrospray, limiting cases for the electrostatic interaction energy are considered first. For the limit of two nonpolarizable point charges the electrostatic interaction energy is given as[26]

$$U^0 = K\frac{Q_1 Q_2}{h} \tag{3}$$

This is the usual Coulomb relationship, which is entirely repulsive for two like-charged particles and has been used extensively in models of the behavior of highly charged droplets. From a second limiting case, namely a point charge interacting with a polarizable sphere, it is possible to identify induced multipole terms that contribute to the electrostatic interaction. For a point charge of Q_1, interacting with a sphere of radius a_2 and dielectric constant ε_2 the electrostatic interaction energy is given by[31]

$$U^1 = K\frac{Q_1 Q_2}{h} - \frac{KQ_1{}^2}{2}\sum_{m=1}^{\infty}\frac{(\varepsilon_2 - 1)m}{(\varepsilon_2 - 1)m + 1}\frac{a_2{}^{2m+1}}{h^{2m+2}} \tag{4}$$

For $m = 1-3$, the leading three attractive interactions derived from eq 4 vary as $1/h^4$, $1/h^6$, and $1/h^8$, and these represent the ion-induced dipole, induced quadrupole, and induced octupole polarizabilities that are the normal components of a multipole expansion of induced electrostatic interactions. Subtle differences in the form taken by eq 4 can arise from how the integration limits on the equation for the electrostatic force are defined.[26] In order to correctly describe a Coulomb energy barrier, it is necessary to take limits for integration of the force that define the work performed in moving a charged particle from infinity to a point h, which represents the distance between the charges as they begin to separate. Depending on the balance between the first and second terms to eq 4, U^1, the electrostatic interaction energy, can be either repulsive or attractive. Equivalent dependences on h can be identified from relationships derived by both Linse[28] and Messina[32] for the interaction between a point charge and a dielectric particle. Equation 4 can be identified with an expression for the force,

F_{12}, between a point charge and a polarizable sphere that is equivalent to one given very much earlier by Smythe.[33]

In the limit of $\varepsilon_2 \to \infty$, the geometric series in eq 4 can be evaluated analytically to give eq 5, which is the solution for the image charge model that is used to analyze the interaction between a point charge and a metallic or conducting sphere.[34,35] Equation 5 has also been used to interpret data relating to the electrospray mechanism.[36,37]

$$U_{IC} = K\frac{Q_1 Q_2}{h} - K\frac{Q_1{}^2}{2}\frac{a_2{}^3}{h^2(h^2 - a_2{}^2)} \tag{5}$$

Important differences between eqs 4 and 5 are that for the latter there is now a leading term that varies as $1/h^2$ and eq 5 also has a singularity at $h = a_2$, which does not appear in the dielectric particle model.

IV. RESULTS AND DISCUSSION

Since molecular clusters were first observed in a mass spectrometer, the stability of multiply charged forms has been a subject of considerable interest and speculation.[1,2,23] There have been numerous experimental attempts to observe the process of Coulomb fission, and for molecular clusters, these have not been particularly successful;[1,18] however, charge separation has been observed in photoexcited multiply charged clusters of metal atoms.[38] Last, Jortner and co-workers have complemented the experimental work by attempting to predict the fission pathways of highly charged atomic and molecular clusters.[17]

Coulomb fission in either a cluster or as part of the ESI mechanism can be decomposed into two subprocesses: (i) the breakup of a multiply charged cluster into two closely associated charged fragments and (ii) rapid separation of the fragments driven by electrostatic repulsion. If steps (i) and (ii) are not spontaneous, then the implication is that any delay in Coulomb fission is caused by the presence of a potential energy barrier, which impedes separation of the charges and/or fragments. If fission results in just two fragments, then the Coulomb repulsion that accompanies separation of the fragments should lead to a significant release of kinetic energy, and estimates from previous experiments range from 0.2 to 1 eV.[1,6,38] Apart from earlier studies of triply charged CO_2 and NH_3 clusters,[1,18] neither of which included any size-dependent data, there have been no recorded examples of delayed Coulomb fission of molecular clusters. The failure to observe Coulomb fission on the part of doubly charged clusters has been attributed to a presence of compression modes,[1,39] which when excited by Coulomb repulsion can dissipate large amounts of energy from a cluster via monomer evaporation. A previous study of the collision-induced fragmentation of triply charged benzene clusters showed that excitation promoted charge separation, which was accompanied by extensive neutral molecule loss .[5]

A series of five molecular dication cluster systems have been studied with a view to identifying patterns of behavior close to the Rayleigh instability limit. Figure 1 shows two examples of mass spectra recorded for ammonia and acetonitrile clusters in regions of the m/Q range where dications are starting to emerge as metastable species. The latter classification has been used in order to emphasize the fragile nature of these particular dication clusters. It also recognizes the possibility that these dications may only be stable because of the presence of a barrier created by Coulomb repulsion between the singly
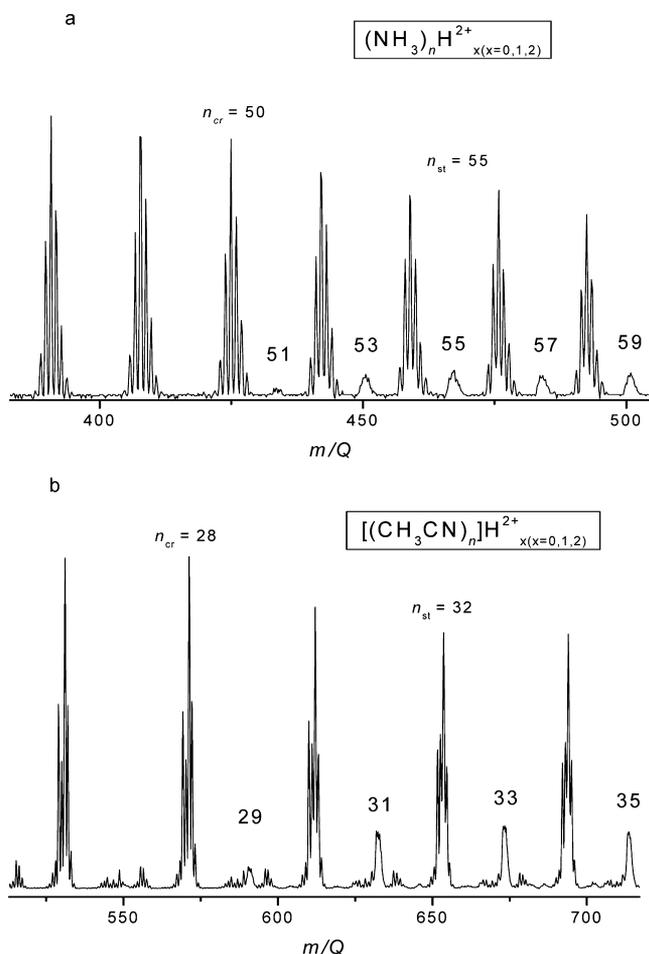
Figure 1. Examples of cluster mass spectra recorded at m/Q ranges where dications become observable. Values for n are given, as are the sizes identified for n_{cr} and n_{st}, the minimum stable size and the size above which the ions no longer exhibit Coulomb fission, respectively. (a) Ammonia clusters, $(NH_3)_n H^{2+}_x$, where x, the number of additional hydrogen atoms, lies between 0 and 2; (b) Acetonitrile clusters, $(CH_3CN)_n H^{2+}_x$, where x, the number of additional hydrogen atoms, lies between 0 and 2.

Table 1. Minimum Stable Size (n_{cr}) Observed for Dication Clusters Composed of Each of the Molecules Listed and the Size (n_{st}), at which the Clusters Become Stable with Respect to Coulomb Fission[a]

molecule	n_{cr}	n_{st}
NH_3	50	55
H_2O	35	40
CH_3CN	28	32
C_6H_6	22	26
C_5H_5N	12	27

[a]All dication lying between n_{cr} and $n_{st} - 1$ were observed to undergo Coulomb fission.

significant contributions from ^{13}C, which will also influence the mass spectra.

Each dication identified from mass spectra, such as those shown in Figure 1, has been selected according to m/Q value and any subsequent unimolecular fragmentation recorded by scanning the electrostatic analyzer to produce a MIKE spectrum. Examples of MIKE spectra from each of the five molecular dications are shown in Figure 2, where it can be seen that most peaks associated with fragmentation exhibit a shape that is characteristic of Coulomb fission.[27] Fragment ions that are expelled parallel and antiparallel to the flight direction of the precursor ion pass through the instrument to be detected; however, the ejection energy is sufficiently high that ions expelled orthogonal to the flight direction are subject to severe instrumental discrimination, which leads to a loss of signal at the center of each profile. In some instances, the centers of profiles do not correspond exactly to the loss of integer numbers of molecules and there is some evidence for the movement of one or two H-atoms between fragments; an obvious example being $(H_2O)_n^{2+}$ which fragments into $[(H_2O)_{n-k-2} \ OH]^+$ and $H_3O^+(H_2O)_k^+$, and in this instance reflects how charges might be accommodated in the precursor cluster.[3] Less obvious examples include the appearance of $(C_6H_6)_k H_2^+$ as a fragment. Since these processes do not influence the interpretation of data, specific instances have not been identified in the MIKE spectra. Within each ion series, for example, $(H_2O)_n^{2+}$ and $(H_2O)_n H_2^{2+}$, the presence or absence of excess protons does not make a significant difference to the fragmentation pattern; however, as n increases there is a shift toward slightly larger values of k. In some case, for example $(C_6H_6)_{24}^{2+}$ where $k = 9$ and 10, there is evidence of more complete peak profiles. Bearing in mind that the larger of the fragments is being detected, these profiles probably correspond to instances where an ion has undergone Coulomb fission to give a fragment where the number of constituent molecules is less than k, and then during the remaining flight time to the ESA additional neutral loss occurs to arrive at k as a total. Because the loss of neutral atoms and molecules from clusters is accompanied by relatively small releases of kinetic energy,[41] there is far less instrumental discrimination and the effect is to "infill" peak profiles. Similar effects can be seen in peak profiles where charge separation in dication clusters has been induced by collisional activation.[6] Since this effect is quite pronounced, it lends confidence to the assumption that distinctly dish-shaped profiles are the result of fragmentation into two intact fragment ions. A further possible source of composite peak profiles is electron capture, which has previously been identified as a charge reduction process in metal dication complexes.[42] However, in the current experiments the pressure in the flight

charged clusters as they start to separate. As can be seen from Figure (1), the point at which dications of an odd size begin to appear is quite distinct; however, an overlap with a more intense series of single charged ions obscures the fact that, in some instances, the minimum stable size, n_{cr}, can be even-valued. In such cases, n_{cr} has been determined by the presence of fragments from Coulomb fission. Since some of the dications appear at half-integer m/Q values, their presence in coincidence with singly charged cluster ions can be seen in figure 1 via the effect they have on mass resolution. Table 1 summarizes n_{cr} values determined for each of the five molecular dications studied here. In some cases, these numbers are one unit lower than those recorded previously because earlier measurements relied on observations from mass spectra rather than fragmentation patterns.[1] For several dications, mass spectra recorded at higher resolution reveal evidence of more than one type of doubly charged ion. For example, $(H_2O)_n^{2+}$ and $(H_2O)_n H_2^{2+}$ have previously been identified by Stace,[2] and experiments by Garvey et al.[40] have shown the presence of $(NH_3)_n^{2+}$, $(NH_3)_n H^+$, and $(NH_3)_n H_2^{2+}$. In addition, those ions containing large numbers of carbon atoms will include

Figure 2. Examples of Coulomb fission recorded for each of the five molecular studied. For size-selected precursor ions fragmentation patterns have been recorded as a function of laboratory-frame kinetic energy using the MIKE technique.[27] Fragments lost by the precursor ion are identified by the label k, and below selected peaks are values determined for the average kinetic energy release that accompanies Coulomb fission. (a) $(H_2O)_{37}^{2+}$, (b) $(NH_3)_{52}H_2^{2+}$, (c) $(C_6H_6)_{24}^{2+}$, (d) $(C_5H_5N)_{18}^{2+}$, and (e) $(CH_3CN)_{31}^{2+}$.

tube of the mass spectrometer is too low for collisions to occur between the dications and a background gas (most probably N_2), and if a collision were to occur then the ionization energy difference between the cluster and N_2 would make electron transfer highly improbable. What Figure 2 also shows is that Coulomb fission can be a very asymmetric process with many of the smaller fragments containing just 20% of the total number of molecules in a cluster. If the observation time window could be reduced, then it is quite possible that evidence for even greater asymmetry in the fragments could be captured.

By investigating individual dications for fragmentation, it has been possible to identify the range for n over which Coulomb fission extends. The upper limit is given as n_{st} in Table 1 and is the size at which a dication cluster ceases to undergo Coulomb fission. As can be seen, for most of the dications, the first four or five members of each series exhibit instability with respect to Coulomb fission; however, for pyridine the range extends over 14 dications. Coulomb fission is not the only fragmentation process the dications exhibit. Figure 3 shows two examples of where dications within the Rayleigh instability range have been
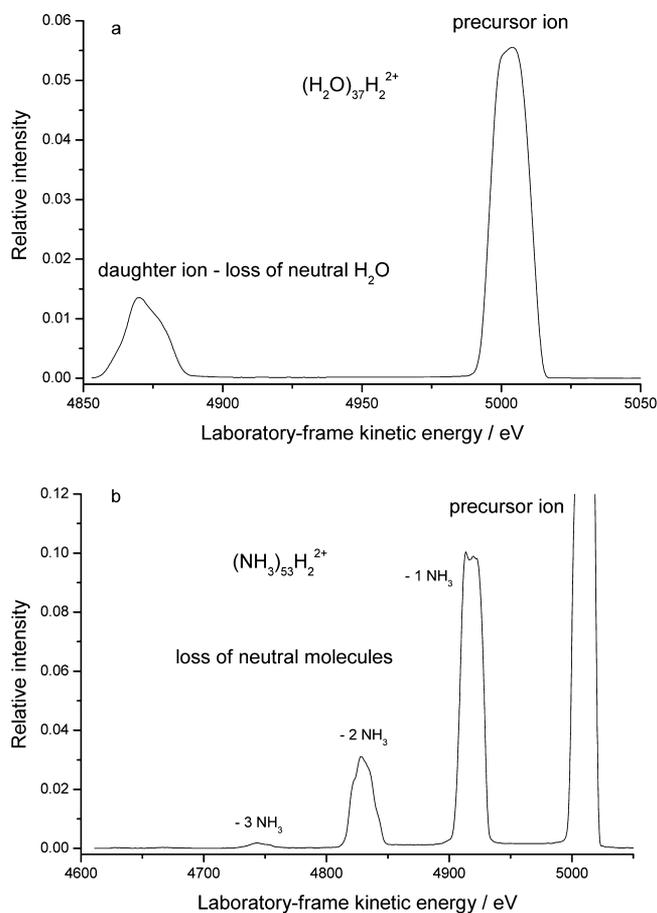
Figure 3. Examples of where ions identified as within the Rayleigh instability limit are also observed to undergo the loss of neutral molecules. Fragmentation patterns have been recorded as a function of laboratory-frame kinetic energy using the MIKE technique.[27] (a) $(H_2O)_{37}H_2{}^{2+}$ and (b) $(NH_3)_{53}H_2{}^{2+}$.

Figure 4. Expanded view of a single peak profile taken from Figure 2a. The peak arises through the loss of $H_3O^+(H_2O)_9$ from $(H_2O)_{37}{}^{2+}$ and due to Coulomb repulsion between the separating fragments, the processes has associated with it a center-of-mass kinetic energy release of approximately 1 eV.

Table 2. Experimental and Calculated Kinetic (Ejection) Energy Data for Selected Dication Clusters[a]

| | | kinetic (ejection) energy $\langle K.E.\rangle$/eV | |
molecular dication	ε_i	experiment	theory
$[(NH_3)_{52}]^{2+}$	22	0.77−1.00	1.01−1.03
$[(H_2O)_{37}]^{2+}$	80	0.91−1.00	1.19−1.23
$[(CH_3CN)_{31}]^{2+}$	39	0.76−0.86	0.88−0.91
$[(C_5H_5N)_{18}]^{2+}$	12	0.69−1.00	0.98[b]
$[(C_6H_6)_{24}]^{2+}$	2.3	0.74−0.80	0.92[b]

[a]The experimental data are presented as a range of values for average kinetic energy releases $\langle K.E.\rangle$ as determined from individual peak profiles present in a given MIKE scan. The calculated results, obtained using the analytical dielectric particle model,[26] show the spread in kinetic energy expected from the size range recorded for the ejected cations. [b]Most of the fragmentation pathways for these ions are predicted not to have barriers arising from electrostatic attraction.

examined for the loss of neutral molecules. As can be seen, at least one of the ions exhibits quite extensive fragmentation, which from the location within the apparatus where these processes are being observed, means that Coulomb fission and neutral loss are both occurring on a time scale of $\sim 10^{-4}$ s. Unfortunately, the relative intensities of the two types of signal, for example, comparing Figures 2a and 3a, are not good indicators of the most probable pathway, because unlike Coulomb fission, neutral loss is not subject to the same high degree of instrumental discrimination. What can be stated with confidence is that Coulomb fission and neutral evaporation are taking place in competition.

From the widths of the peaks in Figure 2 it has been possible to determine the average kinetic energy with which small ions are ejected from the doubly charged clusters.[27] Figure 4 shows an expanded view of a peak profile taken from Figure 2a for the fragment $H_3O^+(H_2O)_9$ from $(H_2O)_{37}{}^{2+}$, from which a kinetic energy release can be estimated from the full-width at half-maximum. Sample values of kinetic energy release are also displayed below some of the profiles in Figure 2, and average values for specific clusters are given in Table 2, where it can be seen that the ejection energies typically lie between 0.7 and 1.2 eV. At first sight these numbers would appear quite reasonable; taking eq 3 and assigning values to all of the constants, the repulsion between two point charges ($Q_1 = Q_2 = 1$) separated by a distance h is given by $U^0 = 1.44/h$, where U^0 is in eV and h

is in nm. From the density of water the diameter of $(H_2O)_{37}{}^{2+}$ is calculated to be ~ 1.3 nm, and since the charges are expected to be as far apart as possible (otherwise there would not be a critical size), a repulsive energy of approximately 1 eV is not unreasonable. However, this simple treatment neglects the dielectric nature of water (and the other solvents) and so the equation should be corrected to $U^0 = 1.437/(h\varepsilon_i)$, where ε_i is the dielectric permittivity of a bulk sample of the molecules that constitute the cluster. For water this value is 80 and therefore, the repulsion between the two charges at 1.3 nm separation is now calculated to be just 0.0125 eV. Under these circumstances, some of the values given in Table 2 would be closer to a situation where the two charges reside on adjacent molecules, but again this would not explain the presence of a critical size. Taken together with the preference for very asymmetric fragmentation there are clearly aspects to these experimental results that cannot be explained by simple point charge electrostatics. Strictly speaking, dielectric permittivity should only be used to describe the behavior of macroscopic amounts of any material. Using the term to account for how a small collection of, for example, water molecules might moderate the effects of an electric field generated by a charge, simply means that ε_i takes the form of a parameter. However, in these calculations ε_i will retain the value attributed to each material in
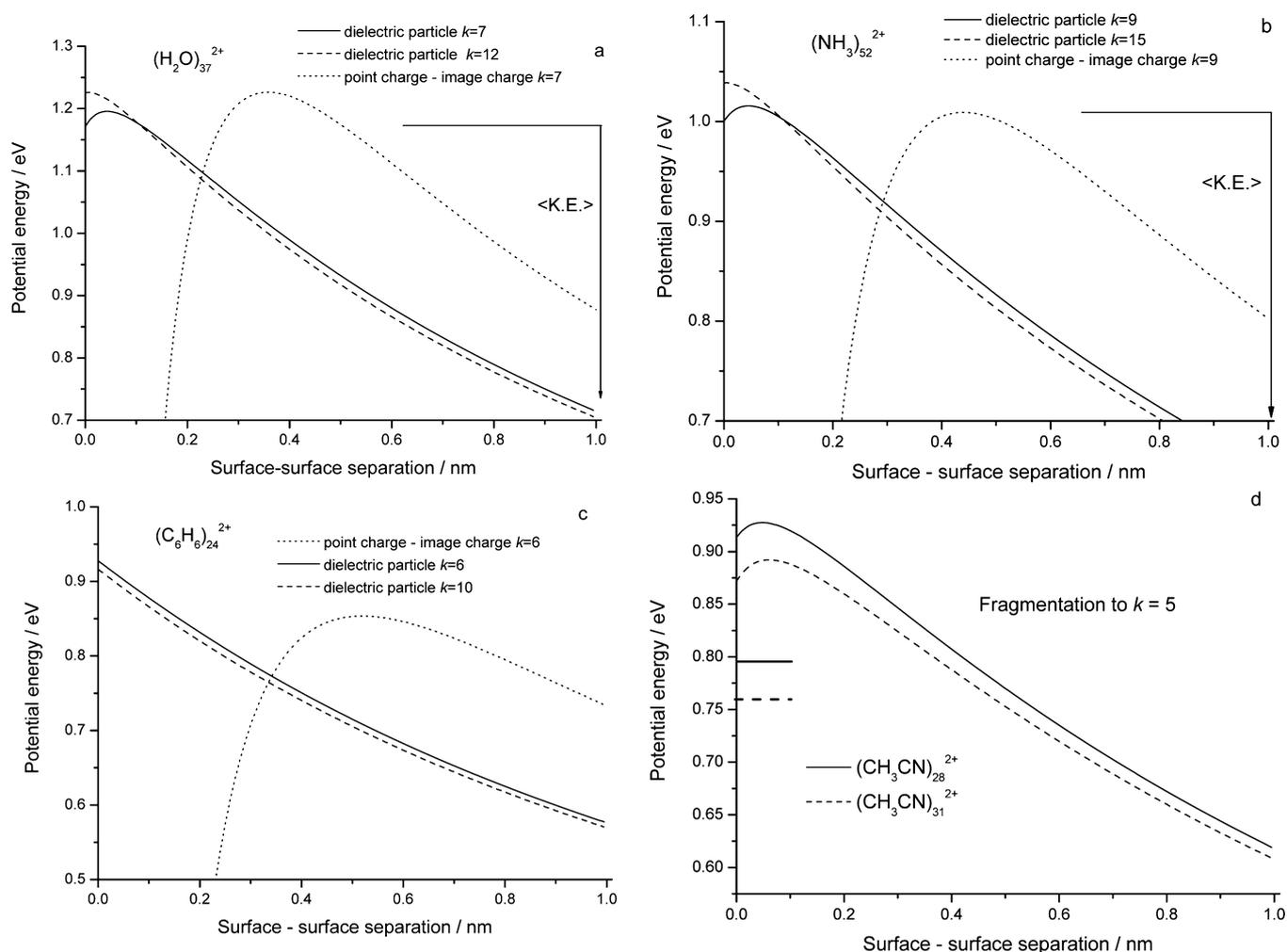
Figure 5. Potential energy curves calculated to represent the reverse Coulomb barrier that arises as individual cluster dications undergo charge separation. The fragment ions are represented in the dielectric particle model as spheres and their dielectric constants and radii are given in Tables 2 and 3, respectively. Also shown are potential energy curves calculated using the point charge–image charge model, eq 5. (a) $(H_2O)_{37}^{2+}$, (b) $(NH_3)_{52}^{2+}$, and (c) $(C_6H_6)_{24}^{2+}$. The values assigned to k span the range of fragments observed for each of these ions. In panel d potential energy curves have been calculated to compare the consequences of either $(CH_3CN)_{28}^{2+}$ or $(CH_3CN)_{31}^{2+}$ losing a $k = 5$ fragment.

the bulk. Similarly, no account has been taken of the known temperature dependences associated with dielectric constants, particularly as we have no detailed knowledge of the internal temperatures of the dication clusters. Taking water as an example, for the results discussed below there were no significant differences between taking a dielectric constant appropriate for ice and that for warm water. Were a calculated difference could arise is when the dielectric constant is small and a change of temperature causes a significant increase or decrease; however, existing experimental data on benzene, for example, shows that not to be the case.[43]

In order to better understand the factors responsible for high fragment kinetic energies and asymmetric fragmentation patterns, use has been made of the solution to eq 2 to calculate potential energy curves for the initial step in the separation of two charged dielectric spheres. Results corresponding to two possible fragmentation pathways for each of the clusters $[(H_2O)_{37}]^{2+}$, $[(NH_3)_{52}]^{2+}$, and $[(C_6H_6)_{24}]^{2+}$ are given in Figure 5, where the calculations have used the radii (a_1 and a_2) given in Table 3 and the dielectric constant data presented in Table 2. These potential energy curves, which have been calculated from the analytical dielectric particle

model, are significant for several reasons. First, the barriers are not all completely repulsive; some show the presence of a short-range attraction between the two fragments that is influenced by their relative sizes. The effect of the attraction is to reduce the magnitude of the reverse electrostatic barrier, which in turn favors asymmetric fragmentation. Second, the height of a barrier with respect to infinite separation of the spherical particles provides an upper limit to the magnitude of the kinetic (ejection) energy. For selected examples of dications, this energy has been calculated over the range of fragmentation pathways they display, and the results are then compared in Table 2 with average values determined from peak profiles for those same ions. As can be seen, for four of the dications there is some overlap between the bounds determined by theory and the experimental results. An obvious source of experimental error is the accuracy with which the width of a given peak can be measured, and the well-defined peaks recorded for $[(H_2O)_{37}]^{2+}$ will clearly provide more accurate results than those, for example from $[(C_5H_5N)_{18}]^{2+}$, where the signal-noise ratio is not so good. In an earlier study the model also provided very good agreement with experimental data on kinetic energy release following the Coulomb fission of highly

Table 3. Size Parameters Used in the Calculation of Potential Energy Profiles for the Separation of Two Singly Charged Fragments from the Process: $(X)_n^{2+} \rightarrow Y^+_{n-2-k} + Z_k^+$[a]

n	k	a_1/nm[b]	a_2/nm[b]
		$(H_2O)_n^{2+}$	
37	7	0.386	0.591
37	12	0.453	0.555
		$(NH_3)_n^{2+}$	
52	9	0.443	0.713
52	15	0.517	0.677
		$(C_6H_6)_n^{2+}$	
24	6	0.626	0.843
24	10	0.730	0.771
		$(CH_3CN)_n^{2+}$	
28	5	0.501	0.768
31	5	0.501	0.802
		$(C_5H_5N)_n^{2+}$	
18	4	0.745	0.543
18	7	0.683	0.635

[a]Some of these energy profiles are shown in Figure 5. [b]Calculated from the density with no allowance for packing fraction.

charged fullerenes to give loss of C_2^+ and C_4^+.[30] The results showed that, even for fragment ions as small as the latter, mutual polarization of the fission products as they separated had a significant influence on the height of the Coulomb barrier.

Two obvious sources of mis-match between theory and experiment can be identified. First, there is the assumption that the separating ions are spherical when in close proximity, and both experiment and theory show this not to be the case.[8,9,12,44] However, molecular dynamics simulations do show the charged products becoming quasi-spherical within a few hundred picoseconds of separation.[44] Second, no account is taken of the possibility that some fraction of the Coulomb energy might be partitioned into internal energy of the cluster fragments. Such an effect could correspond, for example, to the excitation of cluster compression modes as proposed by Gay and Berne.[39] Previous experiments have shown that the excitation of doubly- and triply charged cluster ions through collisional activation can result in very extensive fragmentation, which includes both charge transfer and neutral loss.[4−6] If in the examples discussed here, internal excitation from Coulomb repulsion were to promote additional loss of neutral molecules then evidence of energy partitioning would take the form of composite peak profiles where the central section of each "dish-shaped" profile becomes subject to "infill". Such an effect has already been discussed above, and the $k = 9$ and 10 peaks of the $(C_6H_6)_{24}^{2+}$ MIKE scan are good examples of where additional fragmentation does contribution to a distortion of the primary dish-shape. The MIKE scans for $(C_5H_5N)_{18}^{2+}$ and $(CH_3CN)_{31}^{2+}$ also show similar evidence of having been affected by additional neutral loss. From the data in Table 2, it would appear that approximately 10% of the Coulomb energy is being partitioned into internal excitation of the cluster fragments.

In order to examine further the significance of asymmetric fragmentation, an additional calculation has been undertaken where the behavior of $(CH_3CN)_{28}^{2+}$ and $(CH_3CN)_{31}^{2+}$ has been compared with respect to a single decay channel ($k = 5$). The result is shown in Figure 5d where it can be seen that

asymmetric fragmentation to the $k = 5$ fragment becomes energetically more favorable as the precursor ion increases in size. Also shown in Figure 5d as horizontal lines are experimental kinetic energies recorded for the $k = 5$ fragments from each of the two precursor ions. Although the individual experimental values are, for reasons discussed above, less than the calculated results, their relative magnitudes match those of the calculated barrier heights. A final point regarding the potential energy curves that have been calculated for dielectric particles, concerns their behavior beyond the distance where there is attraction between the separating particles. For Figure 5a,b it can be seen there is a crossing at approximately 0.1 nm and that Coulomb repulsion increases when fragmentation is more asymmetric. This greater repulsion is consistent with a reduction in radius of one of the products being accompanied by an increase in surface charge density. Note that greater Coulomb repulsion with increasing fragment asymmetry is always the case for benzene cluster ions, Figure 5c, because the fragments are not sufficiently polarizable to create short-range attraction.

An overarching conclusion to be drawn from this comparison between experiment and theory is that large doubly charged collections of molecules mostly favor the ejection of small singly charged solvated ions. This process becomes advantageous because multipole electrostatic interactions create a barrier to charge separation that reduces in magnitude as fragmentation becomes more asymmetric. The underlying reason for this pattern can be seen from a consideration of how the surface charge density behaves as the charged fragments start to separate.[45] Figure 6 show two examples of where the bound surface charge density, in the form of either $2\pi a^2 \sin(\beta)\sigma_b(\beta)$ or $2\pi a^2 \sin(\pi-\beta)\sigma_b(\pi - \beta)$, has been calculated for fragments arising from $(H_2O)_{37}^{2+}$ and where the smaller of the singly charged ions corresponds to either $k = 7$ or 12. In Figure 6a the calculated charge density is given for the large fragment that is left following the loss of either the $k = 7$ or 12 ion. As can be seen, the bound charge density has been polarized to give a region of negative charge density close to the point of contact, and that the density is most negative when the polarizing species is the smaller ($k = 7$) ion. However, this effect is mutual in that charge density on the smaller ion ($k = 7$ or 12) is also subject to polarization, and this is shown in Figure 6b, where it can be seen that, for the $k = 7$ ion, there is a region of enhanced positive charge density close to the point of contact. In contrast, charge density on the $k = 12$ fragment ion changes very little. It has been noted previously that there is a close correspondence between the strength of attraction and the degree of mutual polarization experienced by the surface charge when like-charged particles interact with one another.[45]

Finally, comparisons have been made between potential energy curves calculated using the solution to eq 2 and those obtained using the point charge-image charge model, eq 5. In Figure 5a an electrostatic potential calculated from eq 5 is given for the case where a $k = 7$ ion is ejected from $(H_2O)_{37}^{2+}$; in Figure 5b the example corresponds to a $k = 9$ ion being ejected from $[(NH_3)_{52}]^{2+}$; and in Figure 5c the example corresponds to the $k = 6$ fragment from $[(C_6H_6)_{24}]^{2+}$. In all cases the value of k determines a_2 the radius of the larger fragment. Apart from the result for benzene, the barrier heights predicted by the image charge model are comparable to those calculated from the particle–particle model; however, more serious is the fact that the image charge model severely overestimates the degree of attraction between the separating charges. This enhanced
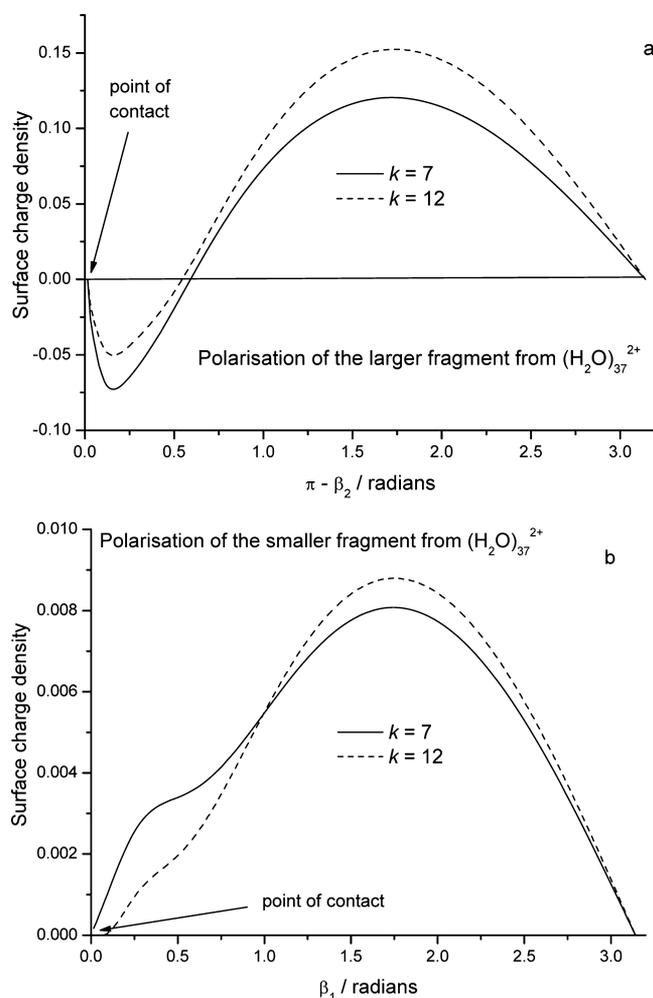
Figure 6. Calculated distribution of bound surface charge density, σ_b, at the point where two fragment ion spheres begin to separate and plotted as a function of polar angle: (a) β_1 for the larger of the fragments from $(H_2O)_{37}^{2+}$ and (b) $\pi - \beta_2$ for the smaller fragment. Results are given for two fragmentation pathways. See ref 41 for details of these calculations.

attraction from eq 5 is most probably due to the $-1/(h^2 - a_2^2)$ term approaching $-\infty$ as the point charge moves closer to the spherical particle. This singularity is prevented in a particle–particle model because both spheres have finite radii.

V. CONCLUSIONS

Molecular dication clusters close to the Rayleigh instability limit have been examined for evidence of charge separation and Coulomb fission. Five separate molecular systems have been studied, and in all cases evidence of Coulomb fission has been found together with the observation that the Rayleigh instability limit extends across a range of sizes. Charge separation is very asymmetric, and Coulomb fission is found to be in competition with neutral evaporation. Values measured for the kinetic energy release following Coulomb fission have been successfully reproduced using a particle–particle dielectric electrostatic model. The close match between theory and experiment supports the view that a majority of the excess charge resides on the surfaces of the particles, which in the case of water matches the conclusion reached from calculations on the structures of protonated clusters.[46]

The calculations present here have also shown how a mutual polarization of bound charge density on separating particles can lead to short-range attraction, which in turn, favors asymmetric fragmentation by lowering the energy barrier to charge separation. It is this aspect of the results that is most closely linked to the ion evaporation mechanism since there are two factors to be taken into consideration. First, as already noted, very asymmetric fragmentation favors a low energy barrier to fragmentation; however, equally important is the polarizability of the solvent. Two of the molecular systems studied, water and acetonitrile, are used as electrospray solvents. Water is good because it is highly polar, which contributes to a lowering of the potential energy barrier to charge separation. However, water is also more dense than acetonitrile, which for the same mass of material makes water droplets smaller and, therefore, less polarizable. As a result, charge separation might be expected to be more effective in acetonitrile because it has droplets that should be more polarizable than those of water. These effects can be seen at work by taking the data in Table 3 and looking at the influence droplet size has on the calculated barriers in Figure 5, panels a and d.

■ AUTHOR INFORMATION

Corresponding Author
*E-mail: anthony.stace@nottingham.ac.uk.

Present Address
†Department of Chemistry, University of Basel, Klingelberg-strasse 80, CH-4056 Basel, Switzerland.

Notes
The authors declare no competing financial interest.

■ REFERENCES

(1) Echt, O.; Kreisle, D.; Recknagel, E.; Saenz, J. J.; Casero, R.; Soler, J. M. *Phys. Rev. A* **1988**, *38*, 3236.
(2) Stace, A. J. *Phys. Rev. Lett.* **1988**, *61*, 306.
(3) Stace, A. J. *Chem. Phys. Lett.* **1990**, *174*, 103.
(4) Gotts, N. G.; Stace, A. J. *Phys. Rev. Lett.* **1991**, *66*, 21.
(5) Gotts, N. G.; Stace, A. J. *J. Chem. Phys.* **1991**, *95*, 6175.
(6) Gotts, N. G.; Lethbridge, P. G.; Stace, A. J. *J. Chem. Phys.* **1992**, *96*, 408.
(7) Mähr, I.; Zappa, F.; Denifl, S.; Kubala, D.; Echt, O.; Märk, T. D.; Scheier, P. *Phys. Rev. Lett.* **2007**, *98*, 023401−1.
(8) Kebarle, P.; Verkerk, U. H. *Mass Spectrom. Rev.* **2009**, *28*, 898.
(9) Crotti, S.; Seraglia, R.; Traldi, P. *Eur. J. Mass Spectrom.* **2011**, *17*, 85.
(10) Grimm, R. L.; Beauchamp, J. L. *Anal. Chem.* **2002**, *74*, 6291.
(11) Smith, J. N.; Flagan, R. C.; Beauchamp, J. L. *J. Phys. Chem. A* **2002**, *106*, 9957.
(12) Kebarle, P.; Pescke, M. *Anal. Chem. Acta* **2000**, *406*, 11.
(13) Hogan, C. J., Jr.; Biswas, P.; Chen, D. *J. Phys. Chem.* **2009**, *113*, 970.
(14) Loscertales, I. G.; de la Mora, F. *J. Chem. Phys.* **1995**, *103*, 5041.
(15) Gamero-Castano, M.; de la Mora, F. *J. Mass Spectrom.* **2000**, *35*, 790.
(16) Gamero-Castano, M.; de la Mora, F. *J. Chem. Phys.* **2000**, *113*, 815.
(17) Last, I.; Levy, Y.; Jortner, J. *J. Chem. Phys.* **2005**, *123*, 154301.

(18) Kreisle, D.; Leiter, K.; Echt, O.; Märk, T. D. *Z. Phys. D: At. Mol. Clusters* **1986**, *3*, 319.

(19) Dole, M.; Mack, L. L.; Hines, R. L.; Mobley, R. C.; Ferguson, L. D.; Alice, M. B. *J. Chem. Phys.* **1968**, *49*, 2240.

(20) Winger, B. A.; Light-Wahl, K. J.; Ogorzalek Loo, R. R.; Udseth, H. R.; Smith, R. D. *J. Am. Soc. Mass Spectrom.* **1993**, *4*, 536.

(21) Iribarne, J. V.; Thomson, B. A. *J. Chem. Phys.* **1976**, *64*, 2287.

(22) Thomson, B. A.; Iribarne, J. V. *J. Phys. Chem.* **1979**, *71*, 4451.

(23) Shukla, A. K.; Moore, C.; Stace, A. J. *Chem. Phys. Lett.* **1988**, *143*, 13.

(24) Chen, X. *Unimolecular Dissociation of Cluster Ions*; Ph.D. Thesis, University of Nottingham: Nottingham, U.K., 2011.

(25) Stace, A. J.; Bernard, D. M.; Crooks, J. J.; Reid, K. L. *Mol. Phys.* **1987**, *60*, 671.

(26) Bichoutskaia, E.; Boatwright, A. L.; Khachatourian, A.; Stace, A. J. *J. Chem. Phys.* **2010**, *133*, 024105.

(27) Cooks, R. G.; Beynon, J. H.; Caprioli, R. M.; Lester, G. R. *Metastable Ions*; Elsevier: Amsterdam, 1973.

(28) Linse, P. *J. Chem. Phys.* **2008**, *128*, 21405.

(29) Wu, G.; Chen, X.; Stace, A. J.; Linse, P. *J. Chem. Phys.* **2011**, *134*, 031103.

(30) Stace, A. J.; Bichoutskaia, E. *Phys. Chem. Chem. Phys.* **2011**, *13*, 18339.

(31) Stace, A. J.; Bichoutskaia, E. *Phys. Chem. Chem. Phys.* **2012**, *14*, 16771.

(32) Messina, R. *J. Chem. Phys.* **2002**, *117*, 11062.

(33) Smythe, W. R. *Static and Dynamic Electricity*, 2nd ed.; McGraw-Hill: New York, 1950.

(34) Redžić, D. V. *Am. J. Phys.* **1994**, *62*, 182.

(35) Stampfli, P. *Phys. Rep.* **1995**, *255*, 1.

(36) Gamero-Castano, M.; de la Mora, F. *Anal. Chem. Acta* **2000**, *406*, 67.

(37) Labowsky, M.; Fenn, J. B.; de la Mora, J. F. *Anal. Chem. Acta* **2000**, *406*, 105.

(38) Bréchignac, C.; Cahuzac, Ph.; de Frutos, M.; Garnier, P.; Kebaili, N. *Phys. Rev. B* **1996**, *53*, 1091.

(39) Gay, J. G.; Berne, B. J. *Phys. Rev. Lett.* **1982**, *49*, 194.

(40) Coolbaugh, M. T.; Peifer, W. R.; Garvey, J. F. *Chem. Phys. Lett.* **1989**, *156*, 19.

(41) Woodward, C. A.; Stace, A. J. *J. Chem. Phys.* **1991**, *94*, 4234.

(42) Wu, B.; Duncombe, B. J.; Stace, A. J. *J. Phys. Chem. A* **2006**, *110*, 8423.

(43) Mardolcar, U. V.; Nieto de Castro, C. A.; Santos, F. J. V. *Fluid Phase Equilib.* **1992**, *79*, 255.

(44) Ahadi, E.; Konermann, L. *J. Am. Chem. Soc.* **2011**, *133*, 9354.

(45) Stace, A. J.; Boatwright, A. L.; Khachatourian, A.; Bichoutskaia, E. *J. Colloid Interface Sci.* **2011**, *354*, 417.

(46) James, T.; Wales, D. J. *J. Chem. Phys.* **2005**, *122*, 134306.